1 **Title: Inactivation mechanism and efficacy of grape seed extract for Human Norovirus**
2 **surrogate**
3
4 Running title: Grape seed extract inactivates Tulane viruses
5
6
7 Chamteut Oh[1,*], Ratul Chowdhury[2,*], Laxmicharan Samineni[3], Joanna L Shisler[4], Manish
8 Kumar[6], and Thanh H. Nguyen[1,5]
9
10 [1]Department of Civil and Environmental Engineering, University of Illinois at Urbana-
11 Champaign, USA
12 [2]Department of Chemical Engineering, The Pennsylvania State University, PA, USA
13 [3]Department of Chemical Engineering, The University of Texas at Austin, Austin, USA
14 [4]Department of Microbiology, University of Illinois at Urbana-Champaign, USA
15 [5]Institute of Genomic Biology, University of Illinois at Urbana-Champaign, USA
16 [6]Department of Civil, Architectural and Environmental Engineering, The University of Texas at
17 Austin, Austin, USA
18
19 *Equal contribution*
20 Corresponding author(s): Thanh H. Nguyen (thn@illinois.edu)
21

22

23

24

25

26

27

28

29

30

31

32

33

34   **Abstract**

35   Proper disinfection of harvested food and water is critical to minimize infectious disease. Grape

36   seed extract (GSE), a commonly used health supplement, is a mixture of plant-derived

37   polyphenols. Polyphenols possess anti-microbial and -fungal properties, but anti-viral effects are

38   not well-known. Here we show that GSE outperformed chemical disinfectants (e.g., free chlorine

39   and peracetic acids) in inactivating Tulane virus, a human norovirus surrogate. GSE induced

40   virus aggregation, an event that correlated with a decrease in virus titers. This aggregation and

41   disinfection was not reversible. Molecular docking simulations indicate that polyphenols

42   potentially formed hydrogen bonds and strong hydrophobic interactions with specific residues in

43   viral capsid proteins. Together, these data suggest that polyphenols physically associate with

44   viral capsid proteins to aggregate viruses as a means to inhibit virus entry into the host cell.

45   Plant-based polyphenols like GSE are an attractive alternative to chemical disinfectants to

46   remove infectious viruses from water or food.

47

48   **Keywords:** polyphenols; grape seed extract; Human norovirus surrogate Tulane virus; virus

49   aggregation; Molecular docking simulations

50

Importance

Human noroviruses are major food- and water-borne pathogens, causing approximately 20% of all cases of acute gastroenteritis cases in developing and developed countries. Proper sanitation or disinfection are critical strategies to minimize human norovirus-caused disease until a reliable vaccine is created. Grape seed extract (GSE) is a mixture of plant-derived polyphenols that is used as a health supplement. Polyphenols are known for antimicrobial, antifungal, and antibiofilm activities, but antiviral effects are not well-known. In studies here, plant-derived polyphenols outperformed chemical disinfectants (e.g., free chlorine and peracetic acids) in inactivating Tulane virus, a human norovirus surrogate. Based on data from additional molecular assays and molecular docking simulations, the current model is that the polyphenols in GSE bind to the Tulane virus capsid, an event that triggers virion aggregation. It is thought that this aggregation prevents Tulane virus from entering host cells.

Introduction

Human noroviruses cause approximately 20% of all cases of acute gastroenteritis in developing and developed countries (1). In the United States, human noroviruses cause about 5.5 million cases of food borne illnesses per year, and about 2 billion dollars in economic loss (2, 3). Noroviruses are transmitted primarily by the fecal-oral route, including ingestion of contaminated food and water or via person-to-person contacts (4). Thus, inactivating human noroviruses present in contaminated food or water is important.

Sodium hypochlorite (NaClO) is regarded as the cheapest and most effective disinfectant to inactivate noroviruses on produce surfaces (5), stainless steel surfaces (6), or in liquid solutions (7). Fresh and fresh-cut produce are generally sanitized with residual chlorine concentrations of 50-200 μg/mL (8). Unfortunately, NaClO is toxic, and produces carcinogenic disinfection by-products (9–11). Thus, both consumers and industry are seeking methods to naturally or minimally process foods with minimal/zero chemical additives (12, 13).

Plants and fruits synthesize polyphenols, chemicals that protect them against damage from external stresses such as infection. Grape seed extract (GSE) is a by-product of grape juice and wine production, and is mass-produced at an affordable price (14, 15). GSE already is sold as an FDA-approved health supplement (16). GSE polyphenols have antimicrobial effects (17) and are considered popular alternatives to chemical disinfectants. GSE possesses anti-viral activity against feline calicivirus (FCV-F9), murine norovirus (MNV-1), bacteriophage MS2, and hepatitis A virus (14, 18, 19). However, the mechanism of virus inactivation is unclear (16). This information is critical because, if GSE is to be used by industries as a natural disinfectant, then researchers must understand how GSE inactivates different types of viruses.

86   The objective of this study was to examine GSE-induced inactivation of Tulane virus, a

87   surrogate for human norovirus. Tulane virus is an ideal surrogate for norovirus because of its

88   structural similarities to human noroviruses (20–22). Thus, Tulane virus has been used to provide

89   more information about potential inactivation of norovirus (7, 23–27). Once GSE disinfection

90   was established, we identified the mechanism of this inactivation using both molecular assays

91   and computer modeling. Studies showed that GSE's main disinfection action occurred due to

92   virus aggregation. Molecular docking simulations identified potential interactions between GSE

93   polyphenols and viral capsids. This study is the first observation that shows plant-derived

94   polyphenols can outperform chemical disinfectants in safely and sustainably controlling water-

95   borne and food-borne pathogens, and also provides the first mechanism for GSE-induced virus

96   inactivation. Thus, GSE may be an attractive disinfectant for industry because of its safety,

97   efficacy and lower impact on the environment.

98

99   **Results**

100   **GSE outperforms chemical disinfectants by 3-log$_{10}$ TV titer reduction**

101   **Fig. 1** shows results from the examination of disinfection properties of GSE against

102   Tulane virus, using a range of different GSE concentrations, Tulane virus (TV) concentrations,

103   and incubation times. For all experiments, GSE was incubated with purified TV. GSE activity

104   was halted by the addition of FBS, and plaque-forming units (PFUs) were quantified as a

105   measure of virus inactivation. We tested GSE concentrations ranging from 42 μg/mL to 678

106   μg/mL because similar GSE concentrations were shown to inactivate other enteroviruses (14, 18,
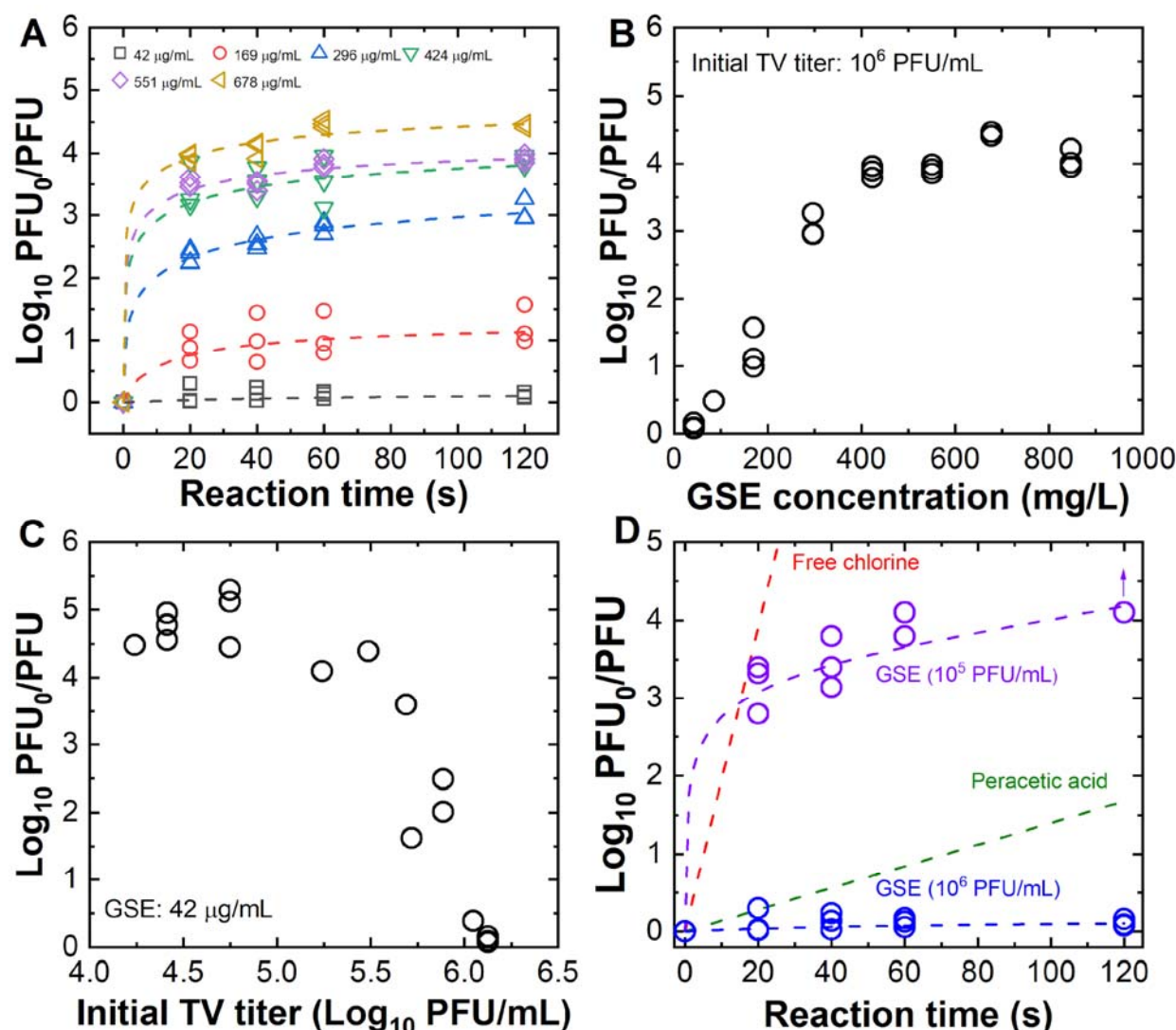
107   19).

108

109

Fig. 1. Inactivation effects of GSE on Tulane virus. 10^6 PFU Tulane virus was incubated with the indicated amount of GSE. FBS was added to quench each reaction at the indicated times. Initial virus titer (PFU_0) was divided by the virus titer at each indicated time (PFU). Thus, the y-axis (Log_{10} PFU_0/PFU) indicates the decrease in virus titer caused by GSE on log_{10} scale. For all experiments, each symbol represents one molecular replicate. **(A)** The dashed lines were trend lines calculated by the pseudo-second-order model. TV inactivation as a function of GSE concentration and time. **(B)** TV inactivation as a function of GSE concentration. In this experiment 10^6 PFU TV was incubated for 120 seconds with the indicated GSE concentrations. **(C)** TV inactivation as a function of GSE concentration. Varying amounts of TV (indicated on the x-axis) were added to reactions containing 42 μg/mL GSE. All reactions were quenched with FBS after a 120 second incubation. **(D)** A comparison of GSE versus peracetic acid and free chlorine inactivation. 10^5 or 10^6 PFU TV was incubated with GSE (42 μg/mL) for 120 sec. The trend lines for GSE were determined by the pseudo-second-order model. The arrow indicates a detection limit. Trend lines for 42 μg /mL free chlorine or peracetic acid were derived by Chick's law with the rate constants determined by our previous studies(7, 27).

125

6

126   TV inactivation increased when GSE concentration and duration of incubation increased

127   (**Fig. 1A**). The inactivation curves were fitted to both the pseudo-second-order model and

128   Chick's law. The correlation coefficients (R^2 values), which reflect the goodness of fit, obtained

129   by the pseudo-second-order model (0.99 to 1.00) were higher than those by the Chick's law (0.34

130   to 0.54) except for the lowest GSE concentration (42 μg/mL) where no significant reduction in

131   virus titers was detected (one-way ANOVA, $p > 0.05$). Parameters from the inactivation kinetics

132   experiments are also listed in **Supplementary Table 1**. The fitting to the pseudo-second-order

133   model showed that it took less than 120 seconds to reach a 95% of $\log_{10}$ PFU reductions at

134   equilibrium state (i.e., $t_{95} < 120$ seconds) for all tested conditions except for the 42 μg/mL case.

135   In **Fig. 1A**, better fitting achieved by the pseudo-second-order model suggested that

136   chemisorption is the dominant reaction between the polyphenols and virus particles (28–30).

137   This finding suggested there were optimal GSE:virion ratios for disinfection, as supported by

138   data in **Fig. 1B** and **1C**. **Fig. 1B** showed that TV inactivation increased as GSE concentrations

139   increased, with GSE efficacy reaching a plateau at 424 μg/mL. This plateau in GSE efficacy

140   shows a maximal number of GSE binding sites on TVs because GSE disinfection could be

141   outcompeted by the addition of TV. **Fig. 1C** showed that GSE disinfection efficiency decreased

142   when more TVs were added to a reaction, supporting the hypothesis that chemisorption occurs

143   between GSE and TV. Interestingly, while 42 mg/mL GSE showed no disinfection activity for

144   10^6 PFU TV (in **Fig. 1A**), it does indeed possess anti-viral properties when lower numbers of TV

145   are present, further supporting the model that GSE polyphenols associate with TV.

146   We compared GSE inactivation rates to those of two commercially available chemical

147   disinfectants (free chlorine and peracetic acid) based on Chick's law and the rate constants

148   obtained from a previous study (27) (**Fig. 1D**). GSE inactivated TV to a 3-$\log_{10}$ virus titer

149   reduction within 16 seconds, a time identical to that of inactivation by free chlorine. In contrast,

150   peracetic acid took much longer (211 seconds) to achieve the same levels of inactivation.

151

152   **GSE causes viral aggregation, and this is likely the main mechanism of GSE-**

153   **induced virus inactivation**

154   **Fig. 1** data showed that GSE inactivated TV, and data suggested that there was

155   chemisorption of GSE to virions. Thus, one possibility is that GSE binds directly to TV to

156   prevent virus-host interactions. **Fig. 2A** quantifies GSE polyphenols in the absence or presence

157   of TV as a means to examine if GSE indeed binds to TV. We incubated 847 μg/mL GSE with

158   10^6 PFU TV. The 2 mL mixture then subjected to ultracentrifugation to separate free versus

159   virus-bound GSE, and GSE in supernatants of samples were quantified. As shown in **Fig. 2A**,

160   there was a statistically significant lower GSE concentration in supernatants when TV was

161   present, implying that GSE indeed binds to TV. Next, we used a light scattering analyzer

162   (DelsaMax Pro, Beckman Coulter) to examine particle size distributions of intact TV and GSE

163   (**Fig. 2B**). Untreated TV showed a polydispersed multimodal size distribution with a major peak

164   at 97 nm and two relatively smaller peaks at 309 and 1755 nm. A single TV virion has a diameter

165   of 40 nm (31), thus most of the TVs in solution were present as dimers, and some populations of

166   viruses were present as timers. Virus populations at 1755 nm were likely multi-virus aggregates.

167   When TV was incubated with 15 μg /ml GSE, there was a shift in the size of the TV peak at 94

168   nm to approximately 300 nm and 1000 nm, implying that this concentration of GSE causes

169   aggregation of TV into trimers and perhaps 10-mers. Experiments using higher concentrations of

170   GSE resulted in greater shifts in sizes, suggesting that GSE is causing TV aggregation. GSE

171   showed a strong single peak at around 1000 nm regardless of GSE concentrations. This peak is

172   believed to represent insoluble polyphenols that are self-aggregated (32). When the GSE

173   solutions were filtered with 0.1 μm filter, the monodispersed peak disappeared from the particle
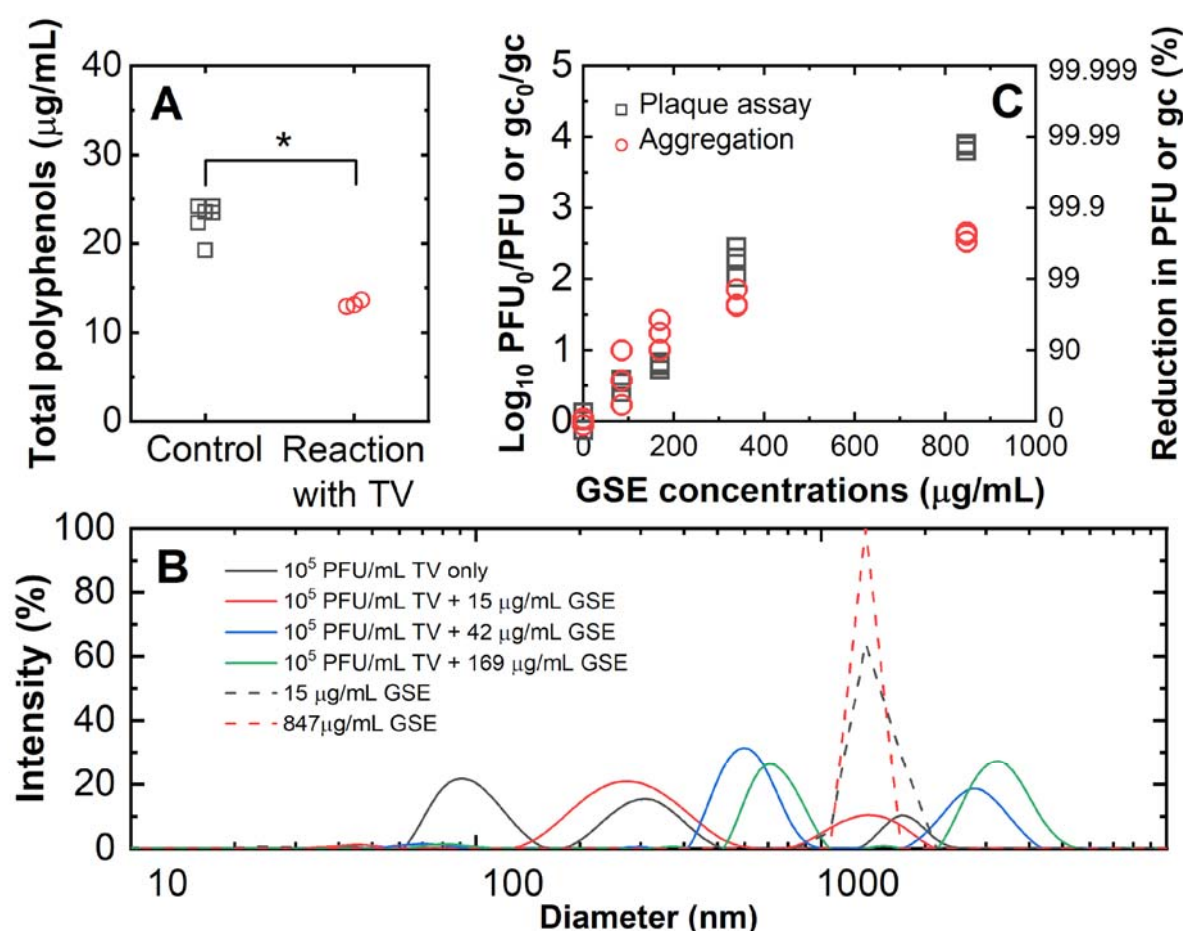
174   size distribution.

175

176

177   **Fig. 2. GSE-induced TV aggregation. (A)** Solutions either lacking (control) or containing 10^6
178   PFU TV were each incubated with 847 μg/mL of GSE followed by ultracentrifugation (150700
179   g) for 3 hours. GSE concentrations were quantified and statistical analysis was performed using
180   the Mann-Whitney test (P<0.05) **(B)** The particle size distribution of TV in the presence or
181   absence of GSE. **(C)** A dose-response curve for plaque and aggregation assays. Plaque assay
182   results were normalized to the initial virus titer and presented in Log_{10} PFU_0/PFU to indicate the
183   decrease in virus titer with different total polyphenol concentrations. Aggregation assay was
184   analyzed by the one-step RT-qPCR and presented in the normalized gene copy number (Log_{10}
185   gc_0/gc) to show the reduction in the number of virions. Equivalent reductions in PFU or gc (%)
186   were also presented on the right y-axis for plaque assay and aggregation assay, respectively. For
187   these experiments, 10^6 PFU TV was incubated with varying concentrations of GSE for 2 minutes

9

188 followed by quenching the reaction with FBS. Each symbol indicates one separate experiment
189 where one plaque assay or three qPCR analyses were conducted.

190

191

192   To further test if GSE induces virus aggregation, virus aggregation and virus titers were

193 quantified in parallel to compare the numbers of virus aggregates and inactivated virus particles

194 after the GSE treatment. For assays shown in **Fig. 2C**, 10^6 PFU TV was incubated with the

195 indicated concentrations of GSE (85 to 847 μg/mL) for 2 minutes followed by quenching the

196 reaction with FBS. Viruses were then either quantified by plaque assay or tested using an

197 aggregation assay. Aggregation assays were designed as follows: untreated or GSE-treated TV

198 were subjected to filtration using a 0.1 μm sized pore filter. Because a single TV virion has a

199 diameter of 40 nm (31), we expect that single and dimeric TV would easily filter through the

200 pore while virus aggregates with three or more virions would be trapped in the filter. Note that

201 our aggregation assay cannot determine a specific number of virions in virus aggregates that can

202 pass through the filter. Viruses that passed through the filter were quantified by one-step RT-

203 qPCR. The ratio of genome copies for untreated versus treated viruses (Log_{10} gc_0/gc) were

204 plotted on the y-axis in **Fig. 2C**. Similar to **Fig. 1**, plaque assays measured virus titers in

205 untreated samples (PFU_0) versus GSE-treated samples (PFU), and data are presented as the ratio

206 of virus titers before and after exposure to GSE (Log_{10} PFU_0/PFU) on the y-axis in **Fig. 2C**.

207 Virus aggregates and plaque were very similar when GSE concentrations below 400 ng/ml were

208 used. However, virus aggregates were significantly lower than inactivated virus titers when 847

209 μg/mL GSE was present. This discrepancy shows the number of virus particles that are larger

210 than 0.1 μm does not fully explain the number of inactivated virus particles determined by the

211 plaque assay. Nevertheless, paired t-test revealed that there was no significant difference

10

212   between the plaque assay and aggregation assay results over the different GSE concentrations

213   (P>0.05). Thus, our current model is that GSE interacts with TV capsid, causing TV aggregation.

214   In turn, aggregation would likely prevent TV from entering host cells. We also demonstrate that

215   GSE aggregation was not reversible; removal of GSE from TV-containing solutions did not

216   make aggregated TV return back into single particle solutions (**Supplementary Text 1**).

217

218   **Molecular docking indicated polyphenols strongly bound to capsid proteins**

219   Data from **Fig. 2** indicated that GSE is physically associated with TV and induced virus

220   aggregation, and that this event likely prevents TV from entering the host cell to begin the virus

221   life cycle. To further investigate this possibility, we conducted molecular docking simulations,

222   an approach that was used to identify interactions between polyphenolic compounds and proteins

223   (33, 34). GSE is a mixture of various polyphenolic compounds (35, 36). We selected nine

224   polyphenolic compounds present in GSE for molecular docking experiments. We chose these

225   compounds based on abundance (36), and this included two phenolic acids (gallic acid and

226   protocatechuic acid), three monomer flavan-3-ols (catechin, epicatechin, and epicatechin

227   gallate), and four dimer flavan-3-ols based on LC-MS analysis (procyanidin B1, B2, B3, and B4)

228   (**Supplementary Table 2**). Although we conducted inactivation experiments using TV, we could

229   not perform molecular docking simulations with the TV capsid because there is no entry for the

230   TV capsid in the Protein Data Bank (PDB, https://www.rcsb.org/). Cryo-EM analysis has shown

231   similarity between the TV and human norovirus (HuNoV) capsids (31), and the HuNoV capsid

232   structure is present in the PBD. Thus, we studied the interaction of the GSE polyphenols with the

233   HuNoV VP1 capsid proteins to understand how GSE may interact with similar TV capsid

234   proteins.

11

235   We performed flexible molecular docking simulations (37, 38) between each of the nine

236   GSE polyphenolic compounds and HuNoV VP1 proteins to discern stable docking

237   conformations, across the four domains of VP1 (S, S-P1 hinge, P1, and P2 domain;

238   **Supplementary Fig. 2**) to identify where each of the polyphenols tended to bind in order of

239   domain preference. For these simulations, we used the HuNoV icosahedral asymmetric unit

240   (PDB ID: 1IHM) that comprised three VP1 proteins because the complete HuNoV capsid

241   consists of 180 identical icosahedral asymmetric units. Residue-level domain definitions have

242   been described by Campillay-Véliz et al. (39). Flexible molecular docking simulations are shown

243   in **Fig. 3**. The expected binding strength of each polyphenol (in increasing order of

244   size/molecular weight) with HuNoV capsid protein has been reported where the error bars

245   indicate variance across top 15 polyphenol binding poses within the same capsid groove. The

246   scale on the right indicates fractional capsid-binding affinity of a given polyphenol with respect

247   to the positive control – BSA. Larger polyphenols tend to show increased affinity towards both

248   the positive control and target capsid of HuNoV. Analysis of binding affinities from docking

249   experiments reveal greater electrostatic stabilization of the larger conjugated electron systems

250   within the bigger polyphenols by the polar grooves of HuNoV capsid and bovine serum albumin

251   alike. Data demonstrated that each of the nine polyphenolic compounds examined from GSE

252   likely bound to different residues or regions of the HuNoV capsid protein. In addition, these

253   polyphenols appeared to bind to a location at the dimeric interface of the trimeric capsid protein.

254   The scores obtained from the simulation reflect the enthalpic contribution of binding (kcal/mol)

255   between the polyphenols and the capsid (40). Fifteen independent trajectories of docking were

256   performed using the docking protocol from OptMAVEn-2.0 suite (38) and the Rosetta energy

257   function (41) was used to score the docked poses. The expected binding score was reported to be

258 the modal value (i.e., most probable score) across the fifteen recorded values per complex. Since

259 the polyphenols tend to show a conjugated electron system, larger polyphenols showed better

260 electrostatic stabilization by the polar binding groove offered by the capsid proteins.

261 Consequently, flavan-3-ol dimers showed stronger binding affinities to the capsid protein than

262 smaller groups of polyphenols (**Fig. 3**). The polyphenol-capsid interaction profiles were

263 composed primarily of hydrogen bonds along with hydrophobic interactions, accounting for the

264 efficient capsid capture seen in experiments (**Fig. 4**). For example, the smallest polyphenol

265 protocatechuate establishes three hydrogen bonded and three hydrophobic contacts while

266 procyanidin (the largest polyphenolic compound) shows up to ten hydrogen bonded contacts yet

267 maintaining the same number of hydrophobic interactions with the capsid (**Supplementary Fig.**

268 **3**). In addition to being concordant with a previous experimental study showing that

269 polyphenols' binding affinity to proteins (e.g., BSA and human salivary α-amylase) increased

270 with their molecular weights (42), we also provide key biophysical insights for the same in this

271 work (**Fig. 4**). Binding affinities for respective polyphenols with the HuNoV capsid were near-

272 equal to that of bovine serum albumin, our positive control (**Fig. 3**). The bovine serum albumin

273 is known as the major protein in FBS (43), with reported quenching activity towards

274 polyphenolic compounds. Thus, our results indicated that the GSE polyphenols tend to promote

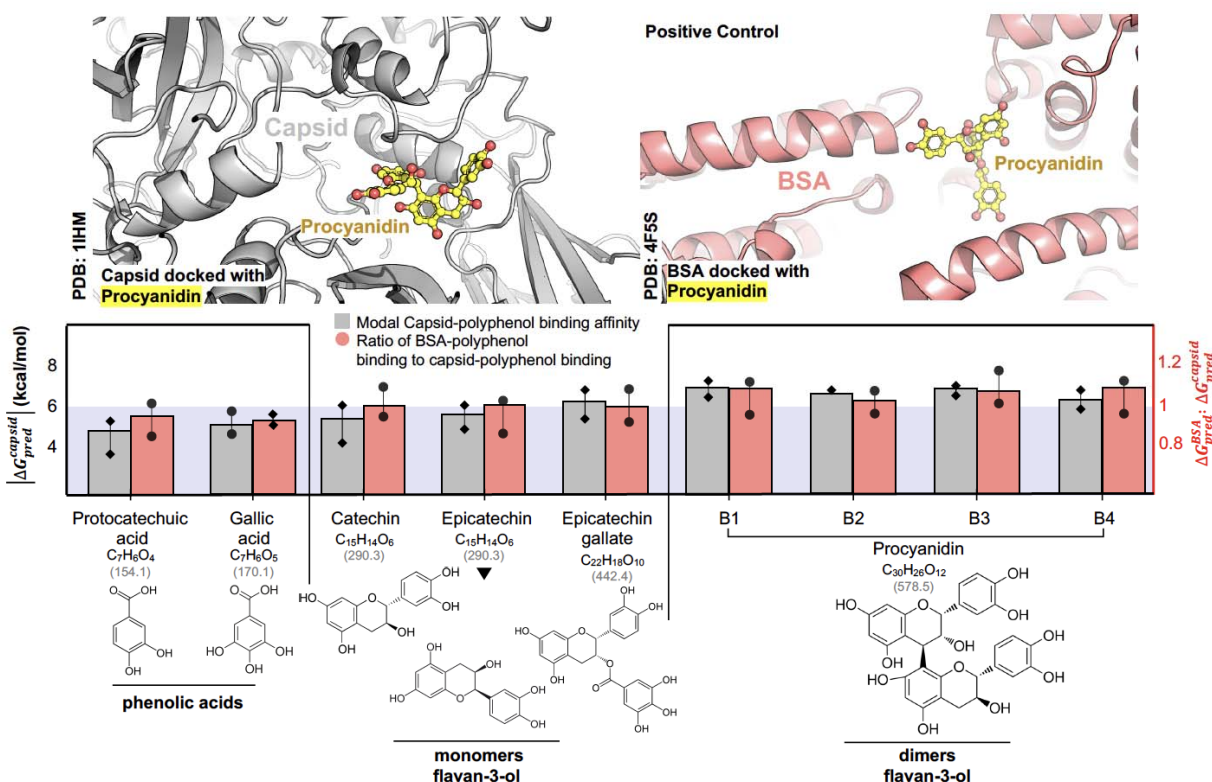275 capture of viral capsids with high efficiency.

276

Fig. 3. Summary of molecular docking analysis between HuNoV capsid and GSE selected polyphenols found in GSE. BSA, which is known to bind strongly with polyphenols (14), was used as a positive control. The expected binding strength of each polyphenol (in increasing order of size/molecular weight) with HuNoV capsid protein (PDB id: 1IHM) has been reported where the error bars indicate variance across top 15 polyphenol binding poses within the same capsid groove. The scale on the right indicates fractional capsid-binding affinity of a given polyphenol with respect to the positive control – BSA.
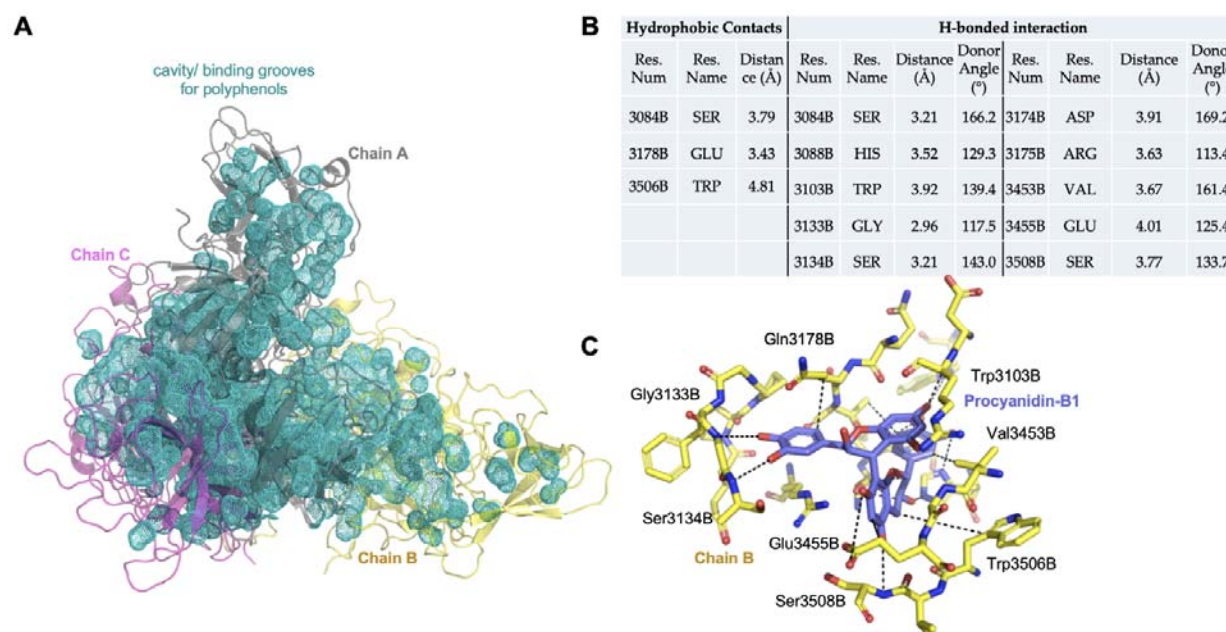
Fig. 4. Larger polyphenols show greater electrostatic stabilization with the viral capsid. **(A)** HuNoV capsid shows a trigonal-symmetric polyphenol accessible groove (indicated in teal), which includes three intra-chain pockets, and three inter-chain binding crevices. Smaller polyphenols can access the inter-chain crevices, while the bigger ones remain localized to the more solvent-exposed intra-chain pockets. **(B)** Residue level interactions of Procyanidin-B1 with the HuNoV capsid are listed. **(C)** A graphical overview of the exact docked pose of Procyanidin-B1 in the capsid groove with most of the interactions is illustrated.

It is noteworthy that as the size of the polyphenol increases, it tends to bind to a less-buried, more solvent exposed pocket (owing to steric clashes) (**Fig. 5**) yet binding to the interface of two chains of the trimeric capsid (located around the S-P1 hinge domain; **Supplementary Fig. 2**). Only the largest Procyanidin (B1-B4) polyphenols cannot access the inter-chain interface pockets and are primarily surface binders with most interactions limited to a single chain (**Fig. 5**). We thereby hypothesize that larger polyphenols tend to be surface binders but stronger capsid binders, while smaller ones preferably bind to inter-chain interfaces of the viral capsid. In terms of domains bound, our docking simulations, in concordance with the experimental data, show that most polyphenols bind to the S or S-P1 hinge domains - while trace binding is observed in the P1 domain and P2 domain is mostly unbound.
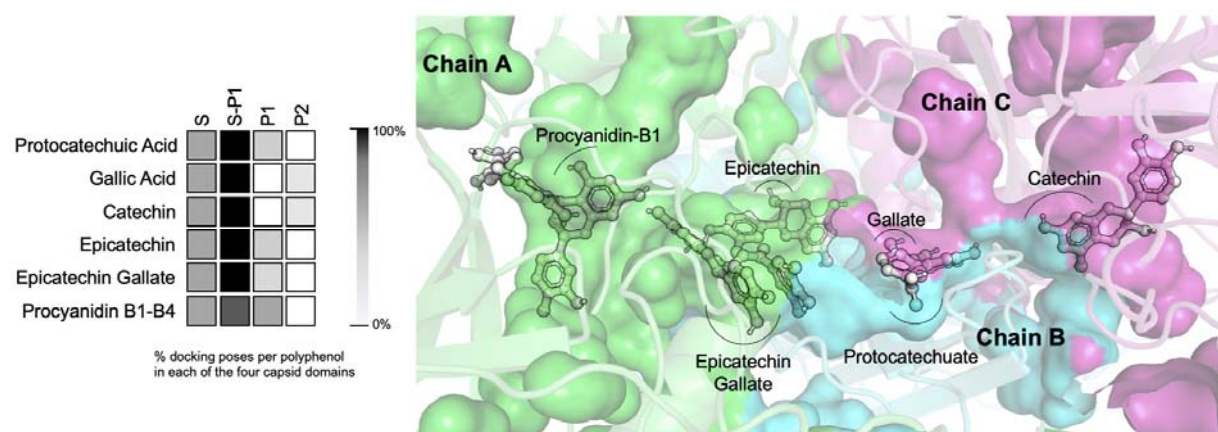
15

306

307

Fig. 5. All polyphenol binding is primarily localized around the S and S-P1 hinge domains of the HuNoV capsid - while the P2 domain remains mostly unbound. Smaller polyphenols can access more buried inter-chain pockets of the HuNoV capsid, while larger Procyanidins bind to surface-exposed pockets with a single chain. Pockets guarded by each chain have been indicated by a different color (green – A, cyan – B, magenta – C). Smaller polyphenols – protocatechuate, gallate, and catechin bind best at the interface of chains B and C. Slightly larger epicatechin and epicatechin gallate bind best at the interface of chain A and B, while larger procyanidins (all B1 through B4) bind best to a solvent-exposed cavity within chain A only.

316

317   We extended the molecular docking simulations to other enteric viruses such as feline

318   calicivirus (FCV-F9), murine norovirus (MNV-1), and hepatitis A virus (HAV) that were

319   experimentally studied in previous works (14, 18, 19). Although the three sets of experiments

320   were performed in different conditions such as different virus media (water or produce) and

321   different pH, they presented a similar trend that FCV-F9 is more susceptible to the polyphenols

322   in GSE than MNV-1 and HAV. Our molecular docking simulation agreed with the experimental

323   data with these enteric viruses. The binding energy of the polyphenols to FCV-F9 capsid protein

324   were stronger than those of MNV-1 and HAV ($P<0.05$) (**Fig. 6**). Note that the binding energy

325   alone will not be sufficient information to evaluate the antiviral effect of the polyphenols because

16

326   the binding energy does not necessarily indicate the following reactions such as viruses being

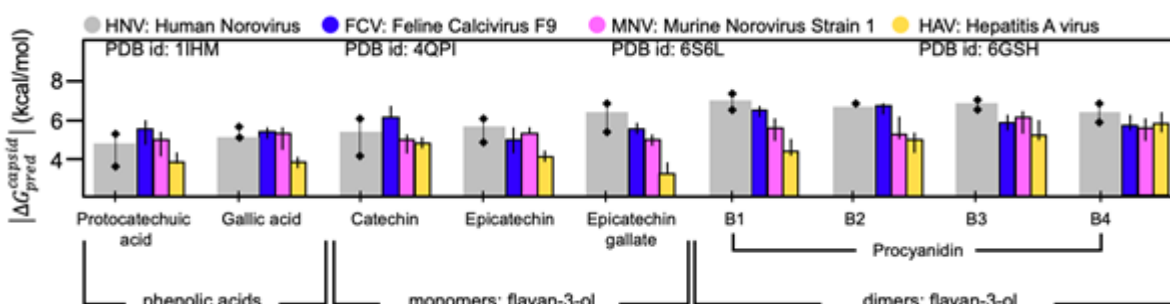327   aggregated and losing infectivity.

328

Fig. 6. Expected binding energies (absolute modal values) between each polyphenolic compound and the four viral capsids (HuNoV: human norovirus, FCV: feline calicivirus F9, MNV: murine norovirus strain 1, and HAV: hepatitis A virus) were computed using the Rosetta binding energy function from top 15 docking poses per complex. The error bars indicate variance from the 15 docked poses for each complex. The reported energy scores were compared by a paired sample t-test indicating a statistically significant higher polyphenol binding activity by HuNoV and FCV in contrast to MNV ($P<0.05$) and HAV ($p<0.001$) capsids.

Discussion

Anti-bacterial, anti-biofilm, and anti-fungal effects of plant-derived polyphenols are well-known. In this study, we systematically evaluated antiviral efficacy of the polyphenols in GSE to TV, a surrogate virus for HuNoV, and the antiviral mechanisms. Data shown here suggest that GSE can inactivate TV and perhaps other enteric viruses. In addition, data show that the polyphenols in GSE aggregate the virus particles, an event that is likely responsible for TV inactivation. Indeed, this concept that TV adsorbs polyphenols was also supported by the binding energy calculated by molecular docking analysis. Our current model is that TV aggregation prevents proper virus-host interactions or virus entry into host cells. There is at least one other report of aggregation of herpes simplex virus, prevents virus entry into cells while allowing virus attachment (44).

17

349   It should be noted that the TV concentrations used in this study are likely much higher

350   than that found in contaminated produce or water. For example, rotavirus concentration in river

351   water, treated wastewater, and untreated wastewater are reported to be $10^{-3.0}$, $10^{-2.2}$, and $10^{-1.3}$

352   FFU/mL respectively (45, 46). Given that GSE was efficacious using these artificially high TV

353   concentrations used in the laboratory, it is reasonable to expect that GSE would be effective as

354   an anti-viral for contaminated food or produce. Also, Tulane virus is more resistant to chemical

355   disinfectants than the other viruses in the *Caliciviridae* family (47). Thus, if GSE were an

356   effective disinfectant of Tulane virus then it is likely GSE would be efficacious against other

357   caliciviruses, and this is an avenue of future research. GSE is also attractive because it is safe for

358   consumption by humans. Thus, GSE or plant-derived polyphenols could be advantageous over

359   the chemical disinfectants for direct addition to end-products that people ingest such as drinking

360   water and foods.

361   There are still several important questions to answer before polyphenols can be widely

362   used to inactivate the water-borne and food-borne pathogens. Water contains other organic

363   matter which could outcompete viruses for binding to polyphenolic compounds. For example,

364   Joshi et al. (14) showed the antiviral efficacy decreased when milk (which has high proteins) was

365   added to an inactivation reaction. Thus, further studies need to be performed to understand how

366   effective GSE is in water that has different properties. Other water properties (e.g., pH, ionic

367   strength, and temperature) are important for adsorption reactions, and additional studies need to

368   address how these properties may affect the efficacy of GSE. If GSE or individual polyphenols

369   were to be used for foods (e.g., apples) then we must also understand how the surface properties

370   of foods (e.g., wax contents of produce surface) may affect the efficacy of GSE (27).

371

Materials and Methods

Commercially available grape seed extract and its plant-derived polyphenols

We purchased a commercial grape seed extract (GSE) solution for this research (7832, Natures plus, USA). The total polyphenol (TP) concentration in each GSE sample was quantified by the colorimetric method using Folin-Ciocalteu reagent. A mixture of 100 μL GSE sample and 500 μL of 10% Folin-Ciocalteu phenol reagent (Sigma-Aldrich, MO, USA) was prepared in a 10 mm path length polymethyl methacrylate (PMMA) cuvette (BrandTech Scientific, CT, USA). Within 3 to 8 min of mixture preparation, 400 μL of 7.5% sodium carbonate solution was added to the mixture and homogenized by pipetting. After incubating at room temperature for 60 minutes, UV absorbance at 765 nm was measured by a spectrophotometer (UV-2450, Shimadzu, Japan). Distilled water was used as a reference solution. The same procedure was conducted with gallic acid solutions with different concentrations prepared by diluting gallic acid monohydrate (Sigma-Aldrich, MO, USA) in distilled water. The TP concentrations of the gallic acid solutions were used for a calibration curve (**Supplementary Fig. 4**) which determined TP concentration of the GSE samples. GSE with TP concentrations ranging from 84 to 1694 μg/mL was prepared by diluting the initial GSE with 1X PBS and used for inactivation experiments.

The polyphenol composition of GSE was analyzed by liquid chromatography-mass spectrometry (Q Exactive™ Plus Hybrid Quadrupole-Orbitrap™ Mass Spectrometer, Thermo scientific, USA), and numerous peaks were discovered by untargeted comprehensive metabolite profiling (**Supplementary Table 2**). Although the LC/MS analysis could not quantify each polyphenol and differentiate polyphenolic isomers with the same m/z values, such as catechin/epicatechin at 291 of m/z ratio for $[M+H]^+$ and B type procyanidins at 579 of m/z ratio for $[M+H]^+$, the major peaks agreed with the primary polyphenolic compounds in GSE that were

395   confirmed by other studies (35, 36). With the mass spectrometry and the references

396   characterizing polyphenols in GSE, we chose nine target polyphenolic components, which

397   include three monomers flavan-3-ols (catechin, epicatechin, and epicatechin gallate), four dimers

398   flavan-3-ols (Procyanidin B1, Procyanidin B2, Procyanidin B3, and Procyanidin B4), and two

399   phenolic acid (gallic acid and protocatechuic acid). These nine polyphenolic compounds were

400   further studied through molecular docking simulations.

401

402   **Tulane virus propagation**

403   Tulane virus (TV) was used as a surrogate for human norovirus (HuNoV). Both TV and

404   HuNoV are members of *Caliciviridae* and share structural similarities. TV and HuNoV have a

405   positive-sense, single-stranded genomic RNA of 6.7 kb and 7.5 kb, respectively. About 23-26%

406   of the genome sequences are identical in both viruses (20). The capsid of TV has T=3

407   icosahedral symmetry and is 40 nm in diameter. The capsid comprises 180 copies of major

408   capsid protein (VP1) or 90 dimers of A/B or C/C. The VP1 is also sub-divided into S, P1, and P2

409   domains. When the VP1 proteins are assembled, the S domains comprise the bottom surface of

410   the capsid while P1 and P2 domains protrude out of the bottom surface, which is responsible for

411   binding to receptor proteins (**Supplementary Fig. 1**). TV recognizes Histo-blood group antigens

412   (21) and sialic acids (22) as cellular receptors similar to HuNoVs. Besides, TV is considered

413   more resistant to disinfectants than the other viruses in *Caliciviridae* (47). Therefore, TV has

414   been widely used in virus inactivation experiments as a surrogate for HuNoVs (7, 23–27).

415   TV was a gift from Cincinnati Children's Hospital Medical Center (22) and the TV

416   genome was sequenced as quality control. The genome sequence was 100% identical to those of

417   a wild-type TV strain in Genbank (Access number: EU391643) (7). TV was propagated in

418 MA104 cells, which was purchased from ATCC (CRL-2378.1), and grown in complete culture

419 medium (i.e., 1X minimum essential medium (MEM; Thermo Fisher Scientific, USA), 10% fetal

420 bovine serum (FBS; Thermo Fisher Scientific, USA), 1X antibiotic-antimycotic (Thermo Fisher

421 Scientific, USA), 17 mM of NaHCO$_3$, 10 mM of HEPES, and 1 mM of sodium pyruvate

422 (Thermo Fisher Scientific, USA). When greater than 90% of MA014 cellular monolayers

423 showed cytopathic effects (about 2 days after the inoculation), cells were harvested and collected

424 by centrifugation, and TV was released from host cells by three cycles of freeze and thaw. Virus

425 was separated from cellular debris by centrifugation at 2000 rpm (556 g) for 10 min (Sorvall

426 Legend RT Plus, Thermo Fisher Scientific, USA). The supernatant was treated by filtration with

427 a 0.22 μm bottle top filter (Milliporesigma, USA) to remove additional cellular debris. The virus-

428 containing filtrate was then further purified using an ultracentrifuge (Optima XPN-90

429 Ultracentrifuge, Beckman Coulter, USA) with a cycle of 1,000 rpm (116 g) for 5 min followed

430 by 36,000 rpm (150700 g) at 4°C for 3 hours. The virus pellet was resuspended in 1X PBS,

431 aliquoted, and stored at -80□ before use.

432

433 **Tulane virus inactivation experiments using GSE**

434 Virus inactivation experiments were initiated by adding 250 μL of TV solution containing 2.5

435 x10^5 PFU TV to 250 μL of GSE-containing solution, in which GSE concentrations ranged from

436 84 to 1694 μg/mL. After the incubation times indicated in the manuscript (i.e., 10 to 120

437 seconds), 70 μL of the mixture was added to 70 μL of FBS to quench the polyphenolic

438 activity(14). Thus, the volumetric ratio of TV, GSE, and FBS in the final solution was 1:1:2. The

439 FBS quenching activity was confirmed in **Supplementary Fig. 5**. Negative controls were

440 prepared for every virus inactivation experiment. In this case, the negative controls were

21

441   prepared by mixing TV, GSE, and FBS in the ratio of 1:1:2, but in a different mixing order.

442   Specifically, 35 μL of GSE was mixed with 70 μL of FBS to quench the polyphenolic activity

443   followed by adding 35 μL of TV to the mixture (**Fig. 1A**). The final mixture of TV, GSE, and

444   FBS was used for further analysis.

445

446   **Plaque assays**

447   The MA104 cell line was grown in 175 cm^2 flasks (Thermo Fisher Scientific, USA) with the

448   complete culture medium. Cells were seeded into 6-well plates (CC7682-7506, USA Scientific,

449   USA) resulting in cellular monolayers with more than 90% confluency. Cell culture supernatants

450   were aspirated using a vacuum-connected pasteur pipette. 100 μL of TV samples were serially

451   diluted by 10-fold dilutions. Cellular monolayers were incubated with each of the serially-diluted

452   viruses for 1 hour at 37□ with 5% CO_2 to facilitate virus attachment to the MA104 cells. Viruses

453   were aspirated from cellular monolayers and 2 mL of overlay solution containing 1X MEM, 1%

454   agarose, 7.5% sodium bicarbonate, 15 mM HEPES, and 1X antibiotic-antimycotic was added to

455   each well. The overlay solution was solidified at 4□ for 10 minutes. Plates were incubated for 2

456   days at 37□ with 5% CO_2 to allow infectious viruses to form plaques. Next, 2 mL of 10%

457   formaldehyde (VWR, USA) in 1X PBS was added to each well and incubated at room

458   temperature for 1 hour to fix cells. The agarose and the formaldehyde were removed and

459   replaced with a 0.05% crystal violet dye solution. The solution was washed away after 10

460   minutes and the number of plaque-forming units (PFU) was counted on a lightbox (ULB-100,

461   Scienceware). The detection limit of the plaque assay was one plaque on the least diluted sample

462   (i.e., 10-fold dilution), which was equivalent to $10^{1.1}$ PFU/mL.

463

464 **Models for virus inactivation kinetics**

465 TV inactivation kinetics were interpreted by a first-order reaction of Chick's law (Eqs. 1-3) and

466 pseudo-second-order model (Eqs. 4-6). Chick's law assumes the activity (i.e., concentration) of

467 available disinfectant remains constant during the reaction. Chick's law has been widely used to

468 describe virus inactivation kinetics by free chlorine, peracetic acid, monochloramine, heat,

469 ozone, and UV(7, 48–51).

470

471 $\frac{dN}{dt} = -kcN$ (Eq. 1)

472 $ln\frac{N}{N_0} = -kct$ (Eq. 2)

473 $log_{10}\frac{N_0}{N} = k'ct$ (Eq. 3)

474

475 Where N referred to viral infectivity (PFU/mL), c indicated the TP concentration (μg/mL), t was

476 treatment time (s), k' meant an inactivation rate constant from Chick's law (L/μg·s).

477 The pseudo-second-order model has been widely used to describe reactions where

478 chemisorption between adsorbent and adsorbate is the rate-determining step (28). In this study,

479 TV and TP were considered as adsorbate and adsorbent, respectively.

480

481 $\frac{dC_t}{dt} = k_2(C_e - C_t)^2$ (Eq. 4)

482 $\frac{t}{C_t} = \frac{1}{C_e^2 k_2} + \frac{1}{C_e}t$ (Eq. 5)

483 $t_{95\%} = \frac{19}{C_e k_2}$ (Eq. 6)

484

23

485   Where t is the reaction time (s), k_2 is the rate constant from the pseudo-second-order model

486   (mL/PFU·s), C_t and C_e are inactivated TV concentration (PFU/mL) at time t and equilibrium

487   state, respectively. Also, $t_{95\%}$ is a reaction time at which C_t reaches 95% of C_e.

488

489   **Virus particle size**

490   The particle size distribution of TV was measured by a light scattering analyzer

491   (DelsaMax Pro, Beckman Coulter). TV, GSE, and FBS either alone or in combination were

492   prepared in 200 μL aliquots, placed in a PMMA cuvette (BrandTech Scientific, USA). Particle

493   size was measured 20 times for each sample, and the averaged % intensity was presented with

494   the particle diameter. According to the manufacturer, particle size analysis is reliable within a

495   range from 0.4 to 10,000 nm, and all our measurements were in this detection range.

496

497   **Virus aggregation assay**

498   An assay was developed to quantify TV virions that are less than 100 μm in diameter. After the

499   TV inactivation experiments were conducted, the mixture containing viruses, GSE, and FBS was

500   filtered with a 0.1 μm syringe filter (Sartorius, Germany). The number of virus particles in the

501   initial mixture and the filtrate was quantified by one-step RT-qPCR. RNA was extracted from

502   samples using Viral RNA Mini Kit (QIAGEN, Germany) in a final 60 μL volume. RT-qPCR

503   samples were prepared in 96-well plates (4306737, Applied Biosystems, USA) by mixing 5 μL

504   of $2 \times$ iTaq universal SYBR green reaction mix, 0.125 μL of iScript reverse transcriptase from

505   the iTaq universal SYBR green reaction mix (Bio-Rad Laboratories, USA), 3 μL of the RNA, 0.3

506   μL of 10 μM TV-NSP1-qPCR-F primer, 0.3 μL of 10 μM TV-NSP1-qPCR-R primer, and 1.275

507   μL of nuclease-free water. The one-step RT-qPCR was run using a qPCR system (QuantStudio

508   3, Thermo Fisher Scientific, USA) with the following thermocycle: 10 minutes at 50□ and 1

509   minute at 90□ followed by 40 cycles of 30 seconds at 60□ and 1 minute at 90□. Detailed

510   information for primers and synthetic DNA controls is summarized in **Supplementary Table 3**.

511   We obtained a calibration curve by plotting the viral infectivity (Log_{10} PFU/mL) on the x-axis

512   and the outcome of the one step RT-qPCR assay (Log_{10} gc/mL) on the y-axis for the same viral

513   solution (**Supplementary Fig. 6**). The calibration curve was used to determine the reliable range

514   of the binding assay. The calibration curve for the binding assay was linear (a slope=0.95 and

515   R^2=1.00) between 10^3 and 10^7 PFU/mL. The PCR standard curves were obtained with 10-fold

516   serial dilutions of the synthetic DNA oligonucleotide (Integrated DNA technologies, USA) and

517   the PCR efficiency for this one-step RT-qPCR ranged from 85 to 95% (R^2>0.99). Inhibitory

518   effect of GSE was also tested (**Supplementary Fig. 7**). We found 100-fold dilution can reduce

519   the inhibitory effect of GSE to an insignificant level, so the samples were diluted in molecular

520   grade water by 100-fold before the RT-qPCR analysis. Information for RT-qPCR was

521   summarized following the MIQE guidelines (52) in **Supplementary Table 4**.

522

523

524   **Molecular docking simulation for polyphenols and capsid proteins interaction**

525   We selected nine polyphenolic compounds that are present in GSE, including two

526   phenolic acids, three monomer flavan-3-ols, and four dimer flavan-3-ols (36). The structural

527   information on the polyphenols were obtained from PUBChem

528   (https://pubchem.ncbi.nlm.nih.gov/). Although we conducted inactivation experiments with

529   Tulane virus, we obtained HuNoV capsid protein instead of TV from the Protein Data Bank

530   (PDB, https://www.rcsb.org/) to study interactions with the polyphenols because the database of

531   PDB does not provide TV capsid information. Cryo-EM structure analysis showed that the TV

532   capsid structure closely resembles that of HuNoV(31).

533   We downloaded the HuNoV icosahedral asymmetric unit (PDB ID: 1IHM) which is a

534   basic building block for the HuNoV capsid. This icosahedral unit comprised three VP1 proteins

535   (i.e., chain A, B, and C in PDB format). The complete HuNoV capsid consists of 180 identical

536   icosahedral asymmetric units. We also used a deep-learning-based structure prediction tool -

537   trRosetta(53), to predict the 3D-structure of the TV capsid (**Supplementary File 1**) from its

538   sequence and a multiple-sequence alignment of related sequences. We studied molecular docking

539   of the polyphenols to HuNoV and to other different enteric viruses including hepatitis A virus

540   (PDB: 4QPI), murine norovirus-1 (PDB: 6S6L), and feline calicivirus-F9 (PDB: 6GSH). Bovine

541   serum albumin (BSA) is a major component for FBS, and BSA showed a strong binding affinity

542   to the polyphenols as confirmed by the quenching effect in the virus inactivation experiments.

543   BSA (PDB: 4F5S) was used as a positive control for molecular docking with the polyphenolic

544   compounds. Next, we used the target proteins (capsids or BSA) and flexible conformations of all

545   the aforementioned nine polyphenol ligands to discern stable docking conformations, record

546   binding affinity scores, and report across four capsid domains where each of the polyphenols

547   tend to bind in order of domain preference. The flexible docking protocol is similar to the Z-

548   Dock protocol(37) as implemented within OptMAVEn-2.0(38).

549

550   **Statistical analysis**

551   All experiments were repeated three times with distinct virus samples (i.e., three biological

552   replications), each of which was analyzed by three separate RT-qPCR measurements (i.e., three

553   technical replications). Paired sample t-test was used to compare results of plaque assay and

26

554   aggregation assay in **Fig. 2C** and binding energies of different viral species (HuNoV, FCV,

555   MNV, and HAV) to polyphenolic compounds in **Fig. 6**. We confirmed that all data for statistical

556   analysis satisfied assumptions of paired sample t-test (i.e., no outliers and normality). For

557   example, all data for statistical analysis were between Q1-1.5IQR and Q3+1.5IQR range, which

558   means there were no outliers. Also, differences between two data sets (e.g., plaque assay versus

559   aggregation assay in **Fig. 2C** or HuNoV versus MNV or HAV in **Fig. 6**) were normally

560   distributed (P>0.05).

561

562   **Acknowledgement**

566

References

1. Ahmed SM, Hall AJ, Robinson AE, Verhoef L, Premkumar P, Parashar UD, Koopmans M, Lopman BA. 2014. Global prevalence of norovirus in cases of gastroenteritis: A systematic review and meta-analysis. Lancet Infect Dis 14:725–730.

2. Scallan E, Hoekstra RM, Angulo FJ, Tauxe R V., Widdowson MA, Roy SL, Jones JL, Griffin PM. 2011. Foodborne illness acquired in the United States-Major pathogens. Emerg Infect Dis 17:7–15.

3. Burke RM, Mattison CP, Pindyck T, Dahl RM, Rudd J, Bi D, Curns AT, Parashar U, Hall AJ. 2020. Burden of Norovirus in the United States, as Estimated Based on Administrative Data: Updates for Medically Attended Illness and Mortality, 2001–2015. Clin Infect Dis https://doi.org/10.1093/cid/ciaa438.

4. BITLER EJ, MATTHEWS JE, DICKEY BW, EISENBERG JNS, LEON JS. 2013. Norovirus outbreaks: a systematic review of commonly implicated transmission routes and vehicles. Epidemiol Infect 141:1563–1571.

5. Fraisse A, Temmam S, Deboosere N, Guillier L, Delobel A, Maris P, Vialette M, Morin T, Perelle S. 2011. Comparison of chlorine and peroxyacetic-based disinfectant to inactivate Feline calicivirus, Murine norovirus and Hepatitis A virus on lettuce. Int J Food Microbiol 151:98–104.

6. GIRARD M, NGAZOA S, MATTISON K, JEAN J. 2010. Attachment of Noroviruses to Stainless Steel and Their Inactivation, Using Household Disinfectants. J Food Prot 73:400–404.

7. Fuzawa M, Araud E, Li J, Shisler JL, Nguyen TH. 2019. Free Chlorine Disinfection Mechanisms of Rotaviruses and Human Norovirus Surrogate Tulane Virus Attached to

590   Fresh Produce Surfaces. Environ Sci Technol 53:11999–12006.

591 8.   Chen X, Hung YC. 2016. Predicting chlorine demand of fresh and fresh-cut produce based

592   on produce wash water properties. Postharvest Biol Technol 120:10–15.

593 9.   Parish ME, Beuchat LR, Suslow T V., Harris LJ, Garrett EH, Farber JN, Busta FF. 2003.

594   Methods to reduce/ eliminate pathogens from fresh and fresh-cut produce. Compr Rev

595   Food Sci Food Saf 2:161–173.

596 10.   Soto Beltran M, Jimenez Edeza M, Viera C, Martinez CI, Chaidez C. 2013. Sanitizing

597   alternatives for Escherichia coli and Salmonella typhimurium on bell peppers at household

598   kitchens. Int J Environ Health Res 23:331–341.

599 11.   Matulonga B, Rava M, Siroux V, Bernard A, Dumas O, Pin I, Zock JP, Nadif R, Leynaert

600   B, Le Moual N. 2016. Women using bleach for home cleaning are at increased risk of

601   non-allergic asthma. Respir Med 117:264–271.

602 12.   Cleveland J, Montville TJ, Nes IF, Chikindas ML. 2001. Bacteriocins: Safe, natural

603   antimicrobials for food preservation. Int J Food Microbiol. Elsevier.

604 13.   Devlieghere F, Vermeiren L, Debevere J. 2004. New preservation technologies:

605   Possibilities and limitations, p. 273–285. *In* International Dairy Journal. Elsevier.

606 14.   Joshi SS, Su X, D'Souza DH. 2015. Antiviral effects of grape seed extract against feline

607   calicivirus, murine norovirus, and hepatitis A virus in model food systems and under

608   gastric conditions. Food Microbiol 52:1–10.

609 15.   Market analysis report. 2019. Polyphenols Market Size, Share & Trends Analysis Report

610   By Product (Grape Seed, Green Tea, Cocoa), By Application (Beverages, Food, Feed,

611   Dietary Supplements, Cosmetics), And Segment Forecasts, 2019 - 2025.

612 16.   Memar MY, Adibkia K, Farajnia S, Kafil HS, Yekani M, Alizadeh N, Ghotaslou R. 2019.

613   The grape seed extract: A natural antimicrobial agent against different pathogens. Rev

614   Med Microbiol 30:173–182.

615 17. D'Souza DH. 2014. Phytocompounds for the control of human enteric viruses. Curr Opin

616   Virol 4:44–49.

617 18. Su X, D'Souza DH. 2011. Grape seed extract for control of human enteric viruses. Appl

618   Environ Microbiol 77:3982–3987.

619 19. Su X, D'Souza DH. 2013. Grape seed extract for foodborne virus reduction on produce.

620   Food Microbiol 34:1–6.

621 20. Farkas T, Sestak K, Wei C, Jiang X. 2008. Characterization of a Rhesus Monkey

622   Calicivirus Representing a New Genus of Caliciviridae. J Virol 82:5408–5416.

623 21. Zhang D, Huang P, Zou L, Lowary TL, Tan M, Jiang X. 2015. Tulane Virus Recognizes

624   the A Type 3 and B Histo-Blood Group Antigens. J Virol 89:1419–1427.

625 22. Tan M, Wei C, Huang P, Fan Q, Quigley C, Xia M, Fang H, Zhang X, Zhong W, Klassen

626   JS, Jiang X. 2015. Tulane virus recognizes sialic acids as cellular receptors. Sci Rep 5:1–

627   14.

628 23. Bridges DF, Breard A, Lacombe A, Valentine DC, Tadepalli S, Wu VCH. 2017.

629   Inhibition of Tulane Virus replication via exposure to lowbush blueberry (Vaccinium

630   angustifolium) fractional components. J Berry Res 7:281–289.

631 24. Li X, Huang R, Chen H. 2017. Evaluation of Assays to Quantify Infectious Human

632   Norovirus for Heat and High-Pressure Inactivation Studies Using Tulane Virus. Food

633   Environ Virol 9:314–325.

634 25. Ailavadi S, Davidson PM, Morgan MT, D'Souza DH. 2019. Thermal Inactivation

635   Kinetics of Tulane Virus in Cell-Culture Medium and Spinach. J Food Sci 84:557–563.

636   26.   Araud E, Fuzawa M, Shisler JL, Li J, Nguyen TH. 2020. UV inactivation of rotavirus and

637   tulane virus targets different components of the virions. Appl Environ Microbiol 86:1–12.

638   27.   Fuzawa M, Bai H, Shisler JL, Nguyen TH. 2020. The basis of peracetic acid (PAA)

639   inactivation mechanisms for rotavirus and Tulane virus under conditions relevant for

640   vegetable sanitation. Appl Environ Microbiol 1–47.

641   28.   Ho YS, McKay G. 1999. Pseudo-second order model for sorption processes. Process

642   Biochem 34:451–465.

643   29.   Ho YS, Ng JCY, McKay G. 2001. Removal of lead(II) from effluents by sorption on peat

644   using second-order kinetics. Sep Sci Technol 36:241–261.

645   30.   Ho YS, Ofomaja AE. 2006. Pseudo-second-order model for lead ion sorption from

646   aqueous solutions onto palm kernel fiber. J Hazard Mater 129:137–142.

647   31.   Yu G, Zhang D, Guo F, Tan M, Jiang X, Jiang W. 2013. Cryo-EM Structure of a Novel

648   Calicivirus, Tulane Virus. PLoS One 8:59817.

649   32.   Pianet I, André Y, Ducasse M-A, Tarascou I, Lartigue J-C, Pinaud N, Fouquet E, Dufourc

650   EJ, Laguerre M. 2008. Modeling Procyanidin Self-Association Processes and

651   Understanding Their Micellar Organization: A Study by Diffusion NMR and Molecular

652   Mechanics. Langmuir 24:11027–11035.

653   33.   Islam B, Sharma C, Adem A, Aburawi E, Ojha S. 2015. Insight into the mechanism of

654   polyphenols on the activity of HMGR by molecular docking. Drug Des Devel Ther

655   9:4943–4951.

656   34.   Srinivasan E, Rajasekaran R. 2016. Computational investigation of curcumin, a natural

657   polyphenol that inhibits the destabilization and the aggregation of human SOD1 mutant

658   (Ala4Val). RSC Adv 6:102744–102753.

659   35.   Chedea VS, Echim C, Braicu C, Andjelkovic M, Verhe R, Socaciu C. 2011. Composition

660   in polyphenols and stability of the aqueous grape seed extract from the romanian variety

661   "merlot recas." J Food Biochem 35:92–108.

662   36.   Rodríguez Montealegre R, Romero Peces R, Chacón Vozmediano JL, Martínez Gascueña

663   J, García Romero E. 2006. Phenolic compounds in skins and seeds of ten grape Vitis

664   vinifera varieties grown in a warm climate. J Food Compos Anal 19:687–693.

665   37.   Pierce BG, Hourai Y, Weng Z. 2011. Accelerating protein docking in ZDOCK using an

666   advanced 3D convolution library. PLoS One 6.

667   38.   Chowdhury R, Allan MF, Maranas CD. 2018. OptMAVEn-2.0: De novo Design of

668   Variable Antibody Regions Against Targeted Antigen Epitopes. Antibodies 7:23.

669   39.   Campillay-Véliz CP, Carvajal JJ, Avellaneda AM, Escobar D, Covián C, Kalergis AM,

670   Lay MK. 2020. Human Norovirus Proteins: Implications in the Replicative Cycle,

671   Pathogenesis, and the Host Immune Response. Front Immunol. Frontiers Media S.A.

672   40.   Cosconati S, Forli S, Perryman AL, Harris R, Goodsell DS, Olson AJ. 2010. Virtual

673   screening with AutoDock: Theory and practice. Expert Opin Drug Discov. NIH Public

674   Access.

675   41.   Chaudhury S, Lyskov S, Gray JJ. 2010. PyRosetta: A script-based interface for

676   implementing molecular modeling algorithms using Rosetta. Bioinformatics. Oxford

677   Academic.

678   42.   Soares S, Mateus N, De Freitas V. 2007. Interaction of different polyphenols with Bovine

679   Serum Albumin (BSA) and Human Salivary α-Amylase (HSA) by fluorescence

680   quenching. J Agric Food Chem 55:6726–6735.

681   43.   Johnson M. 2012. Fetal Bovine Serum. Mater Methods 2.

682   44.   Bultmann H, Busse JS, Brandt CR. 2001. Modified FGF4 Signal Peptide Inhibits Entry of

683   Herpes Simplex Virus Type 1. J Virol 75:2634–2645.

684   45.   Lodder WJ, De Roda Husman AM. 2005. Presence of noroviruses and other enteric

685   viruses in sewage and surface waters in The Netherlands. Appl Environ Microbiol

686   71:1453–1461.

687   46.   Rutjes SA, Lodder WJ, Van Leeuwen AD, De Roda Husman AM. 2009. Detection of

688   infectious rotavirus in naturally contaminated source waters for drinking water production.

689   J Appl Microbiol 107:97–105.

690   47.   Cromeans T, Park GW, Costantini V, Lee D, Wang Q, Farkas T, Lee A, Vinjé J. 2014.

691   Comprehensive comparison of cultivable norovirus surrogates in response to different

692   inactivation and disinfection treatments. Appl Environ Microbiol 80:5743–5751.

693   48.   Dunkin N, Weng S, Schwab KJ, McQuarrie J, Bell K, Jacangelo JG. 2017. Comparative

694   Inactivation of Murine Norovirus and MS2 Bacteriophage by Peracetic Acid and

695   Monochloramine in Municipal Secondary Wastewater Effluent. Environ Sci Technol

696   51:2972–2981.

697   49.   Oguma K, Kita R, Sakai H, Murakami M, Takizawa S. 2013. Application of UV light

698   emitting diodes to batch and flow-through water disinfection systems. Desalination

699   328:24–30.

700   50.   Araud E, DiCaprio E, Ma Y, Lou F, Gao Y, Kingsley D, Hughes JH, Li J. 2016. Thermal

701   inactivation of enteric viruses and bioaccumulation of enteric foodborne viruses in live

702   oysters (Crassostrea virginica). Appl Environ Microbiol 82:2086–2099.

703   51.   Dong S, Li J, Kim MH, Park SJ, Eden JG, Guest JS, Nguyen TH. 2017. Human health

704   trade-offs in the disinfection of wastewater for landscape irrigation: Microplasma

33

705   ozonation: Vs. chlorination. Environ Sci Water Res Technol 3:106–118.

706   52.   Bustin SA, Benes V, Garson JA, Hellemans J, Huggett J, Kubista M, Mueller R, Nolan T,

707   Pfaffl MW, Shipley GL, Vandesompele J, Wittwer CT. 2009. The MIQE guidelines:

708   Minimum information for publication of quantitative real-time PCR experiments. Clin

709   Chem 55:611–622.

710   53.   Yang J, Anishchenko I, Park H, Peng Z, Ovchinnikov S, Baker D. 2020. Improved protein

711   structure prediction using predicted interresidue orientations. Proc Natl Acad Sci U S A

712   117:1496–1503.

713